ELSEVIER

Dipole de-excitation near orthogonal conductor surfaces

S.C. Skipsey [a], G. Juzeliūnas [a,b], M. Al-Amri [a,c], M. Babiker [a,*]

[a] *Department of Physics, University of York, Heslington, York YO10 5DD, England*
[b] *Institute of Theoretical Physics and Astronomy of Vilnius University, A. Goštauto 12, 01108 Vilnius, Lithuania*
[c] *Department of Physics, King Khalid University, Abha, P.O. Box 9003, Saudi Arabia*

Abstract

A dipole active emitter radiating, not in free space, but within a homogeneous dielectric near the intersection line of two orthogonal planar conductors bounding the dielectric displays novel emission characteristics. This situation is shown here to give rise to superradiance and subradiance phenomena that are highly sensitive to the dipole orientation (controllable optically), and to the proximity of the emitter to the intersection line. The theory is developed using non-relativistic quantum electrodynamics where the fields are second quantised in terms of modes satisfying the electromagnetic boundary conditions at the conductor surfaces and the interaction Hamiltonian between the emitter and the quantised fields is the familiar form $H_{int} = -\boldsymbol{\mu} \cdot \mathbf{D}/\varepsilon_0$, where $\boldsymbol{\mu}$ is the dipole moment vector and $\mathbf{D}$ is the quantised electric displacement field. The variations of the emission rate with position are displayed for different dipole orientations and the implications of the results for the possibility of using this physical environment for the realisation of scalable architectures for quantum information processing are pointed out.
© 2005 Elsevier B.V. All rights reserved.

1. Introduction

The physics of a quantum mechanical emitter can be modified significantly by the environment in which it is located. Often the modifications arise due to electromagnetic confinement on close proximity to macroscopic bodies, e.g., the surface of a metal or a dielectric, with the emitter located in vacuum, or embedded in a dielectric. The fact that electromagnetic confinement results in the modification of the spontaneous emission rate was first pointed out by Purcell [1] and was first experimentally confirmed by Drexhage [2] for dipole emitters in the vicinity of a planar conductor surface. Subsequently, it was realised that much

---

interesting physics should arise when atoms and molecules interact with electromagnetic fields in a restricted space arising in the context of artificially fabricated material structures. The electromagnetic fields mediating the interaction are not only restricted spatially because they have to satisfy appropriate boundary conditions at material interfaces, but they also often have restricted spectral distributions, depending on the shape and composition of the structure.

Recent years have witnessed considerable advances in the ability to create material structures of almost any desired shape, thanks to modern deposition techniques and lithography at the micro- and nanometre scales. There have also been parallel developments in the ability to perform delicate experiments, with remarkable advances, not just in the detection of the position of single atoms and of molecular centres to nanometre accuracy, but also in the manipulation of their properties using optical techniques [3]. These advances are now capable of revealing a new range of physical phenomena when the typical lengths are less than an optical dipole transition wavelength.

Furthermore, the physics of quantum systems in a restricted space at the nanoscale has acquired a new significance recently with the advent of modern investigations concerned with quantum information processing and storage and quantum computing [4]. Recent experiments by Grangier and co-workers [5,6] employed a nitrogen colour centre in a diamond nanocrystal to perform the first quantum cryptography experiment with a single-photon source. Zoller and co-workers [7–9], on the other hand, envisage dipole–dipole interaction between quantum systems as the essential interaction for the realisation of a two-bit quantum gate – an important element in a quantum computing architecture. However, at the nanoscale, quantum systems can be sufficiently close to material boundaries to be significantly influenced by the spatial restrictions they impose. Recent theoretical work has explored the influence of the proximity of quantum systems to thin films. The effects on level widths and shifts, as well as pair correlation phenomena have been discussed [10]. The context of a single planar material surface and a film are the simplest geometries as far as field confinement is concerned.

In this article, we put forward and explore a significant variant of the geometry involving material interfaces which, remarkably, has not been focused on before, particularly when quantum systems are positioned at nanometre distances from interfaces. The structure in question is one in which the main feature is the intersection line between the planar surfaces of two materials. The possibilities that we can have any material combinations and an arbitrary angle of intersection, demonstrate the generality of this structure. However, the physics becomes particularly transparent in the case of an intersection at a right angle of the planar surfaces of two perfect conductors. Quantum systems localised in the dielectric region outside the conductors within sub-wavelength distances from the surfaces experience physical effects that, to the best of our knowledge, are novel and could be exploited in the design of scalable architectures for quantum information processing and quantum computing.

The region of space focused on here is in the form of a homogeneous dielectric of dielectric constant ε bounded by the planar surfaces of two conductors defined by $x = 0$ and $y = 0$, as depicted in Fig. 1. As shown in this figure, a normal cross-section is taken to lie in the x–y plane, with the intersection line coinciding with the z-axis. The emitter (represented by an arrow in Fig. 1) is characterised by its electric dipole moment $\boldsymbol{\mu}$, of oscillation frequency ω_0, interacting with the electromagnetic modes satisfying the electromagnetic boundary conditions, simultaneously, at the two conductor surfaces. The effective Hamiltonian of the system can be written as

$$H = \hbar\omega_0 \pi^\dagger \pi - \frac{1}{\varepsilon_0} \boldsymbol{\mu} \cdot \mathbf{D}(\mathbf{R}) + H_{\mathrm{f}}, \tag{1}$$

where $\mathbf{D}$ is the electric displacement operator of the field. In the two-level approximation, the internal motion of the emitter involves only two states: $|e\rangle$, of energy E_{e}, and $|g\rangle$, of energy E_{g}, such that $E_{\mathrm{e}} - E_{\mathrm{g}} = \hbar\omega_0$. The operators π and $\pi^\dagger$ are lowering and raising operators for internal states such that $\boldsymbol{\mu} = \langle\boldsymbol{\mu}\rangle_{\mathrm{eg}}(\pi + \pi^\dagger)$. H_{f}
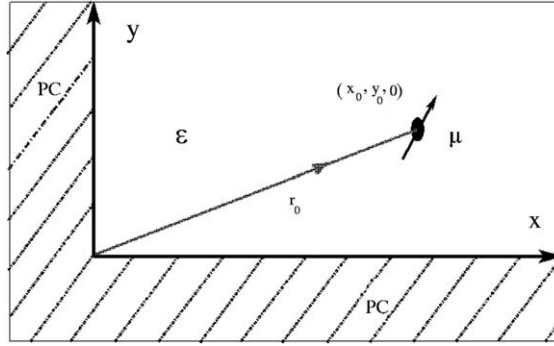
Fig. 1. Schematic arrangement of the region of space occupied by a homogeneous dielectric and the intersection line created by two conducting planes yz and xz at a right angle (shaded regions and referred to as PC). Here, the intersection line is shown along the z-axis, with the emitter situated in the xy-plane, assumed to be fixed at the point $(x_0, y_0, 0)$. The emitter dipole moment vector is shown here pointing at an arbitrary direction.

is the quantised Hamiltonian of the electromagnetic fields in the dielectric region satisfying the usual boundary conditions at the conductor surfaces.

2. Quantised fields

The derivation of the appropriate electromagnetic modes begins with the solutions of the wave equation for transverse electromagnetic fields inside a homogeneous dielectric characterised by its dispersionless dielectric constant ε. There are two types of normal modes: s-polarised (TE) and p-polarised (TM), both of which satisfy the electromagnetic boundary conditions at the planar surfaces of the conductors. The quantised electric displacement field operator **D** is written as follows:

$$\mathbf{D}(\mathbf{R}, t) = \sum_{\eta=(\mathrm{p,s})} \int \mathrm{d}^2\mathbf{k} \int_{-\infty}^{\infty} \mathrm{d}k_z \{ a_\eta(\mathbf{k}, k_z) \mathscr{F}_\eta(\mathbf{k}, k_z, \mathbf{r}, z, t) + \mathrm{h.c.} \}, \tag{2}$$

where h.c. stands for 'Hermitian conjugate' and we have expressed the position vector in components form by writing $\mathbf{R} = (\mathbf{r}, z)$ with $\mathbf{r} = (x, y)$ a two-dimensional (transverse) position vector in the x–y plane. The operator $a_\eta(\mathbf{k}, k_z)$ is the boson annihilation operator for the field mode of polarisation $\eta(=\mathrm{p,s})$ and wavevector components $(\mathbf{k}, k_z)$, where $\mathbf{k} = (k_x, k_y)$ is a two-dimensional wavevector in the positive k_x–k_y quarter-plane. The relevant commutation relations are

$$[a_\eta(\mathbf{k}, k_z), a_{\eta'}^\dagger(\mathbf{k}', k_z')] = \delta_{\eta\eta'}\delta(\mathbf{k} - \mathbf{k}')\delta(k_z - k_z'), \tag{3}$$

$\mathscr{F}_\eta(\mathbf{k}, k_z, \mathbf{r}, z, t)$ are the mode functions for which explicit forms are given below. These transverse vector functions satisfy the wave equation in the dielectric as well as the electromagnetic boundary conditions at the conductor boundaries $x = 0$ and $y = 0$.

The mode functions for the transverse magnetic (TM) modes corresponding to $\eta = \mathrm{s}$ (s-polarised modes) emerge in the form

$$\mathscr{F}_\mathrm{s}(\mathbf{k}, k_z, \mathbf{r}, z, t) = \int \mathrm{d}^2\mathbf{k} \int_{-\infty}^{\infty} \mathrm{d}k_z C(\mathbf{k}, k_z) \left\{ \hat{\mathbf{x}}\frac{k_y}{k} \cos(k_x x)\sin(k_y y) - \hat{\mathbf{y}}\frac{k_x}{k}\sin(k_x x)\cos(k_y y) \right\} \mathrm{e}^{\mathrm{i}(k_z z - \omega t)}, \tag{4}$$

where $k = |\mathbf{k}|$, carets denote unit vectors and the mode normalisation factor $C(\mathbf{k}, k_z)$ is given by

$$C(\mathbf{k}, k_z) = \left(\frac{\varepsilon_0 \hbar \omega}{\pi^3}\right)^{1/2}, \tag{5}$$

where ω is the mode frequency satisfying the dispersion relation

$$\omega^2(k, k_z) = \bar{c}^2 \{ k^2 + k_z^2 \} \tag{6}$$

with $\bar{c} = c/\sqrt{\varepsilon}$.

For the transverse magnetic (TE) modes ($\eta = \mathrm{p}$), we obtain

$$\mathscr{F}_{\mathrm{p}}(\mathbf{k}, k_z, \mathbf{r}, z, t) = \int \mathrm{d}^2 \mathbf{k} \int_{-\infty}^{\infty} \mathrm{d}k_z C(\mathbf{k}, k_z) \left\{ \frac{k_z \bar{c}}{\omega} \left[\hat{\mathbf{x}} \frac{k_x}{k} \cos(k_x x) \sin(k_y y) + \hat{\mathbf{y}} \frac{k_y}{k} \sin(k_x x) \cos(k_y y) \right] \right.$$
$$\left. - \mathrm{i}\hat{\mathbf{z}} \frac{k\bar{c}}{\omega} \sin(k_x x) \sin(k_y y) \right\} \mathrm{e}^{\mathrm{i}(k_z z - \omega t)}. \tag{7}$$

The mode normalisation factor $C(\mathbf{k}, k_z)$, specified in Eq. (5), is fixed by the usual quantisation requirement that the free electromagnetic field Hamiltonian in the dielectric, H_{f}, reduces to the canonical form

$$H_{\mathrm{f}} = \frac{1}{2} \sum_{\eta = (\mathrm{p,s})} \int \mathrm{d}^2 \mathbf{k} \int_{-\infty}^{\infty} \mathrm{d}k_z \hbar \omega \left\{ a_\eta(\mathbf{k}, k_z) a_\eta^\dagger(\mathbf{k}, k_z) + a_\eta^\dagger(\mathbf{k}, k_z) a_\eta(\mathbf{k}, k_z) \right\}. \tag{8}$$

3. De-excitation rate

The de-excitation (or spontaneous emission) rate for an emitter characterised by an electric dipole $\boldsymbol{\mu}$ and which is assumed to be localised at an arbitrary point $\mathbf{R}$ can be evaluated using Fermi's golden rule. By symmetry, this rate cannot depend on the coordinate z, and we may evaluate it for a dipole situated at a general point $(\mathbf{r}_0, 0)$, i.e., at points (x_0, y_0) within the normal cross-section in the x–y plane, as shown in Fig. 1. We have

$$\Gamma(\mathbf{r}_0, 0) = \frac{2\pi}{\varepsilon_0^2 \hbar} \sum_{\eta = (\mathrm{p,s})} \int \mathrm{d}^2 \mathbf{k} \int_{-\infty}^{\infty} \mathrm{d}k_z | \langle \mathrm{e}; \{0\} | - \boldsymbol{\mu} \cdot \mathbf{D}(\mathbf{r}_0, 0) | \mathrm{g}; \{\mathbf{k}, k_z, \eta\} \rangle |^2 \delta(E_{\mathrm{e}} - E_{\mathrm{g}} - \hbar\omega(k, k_z)), \tag{9}$$

where we have represented the de-excitation of the emitter in terms of the transition from an excited state $|\mathrm{e}\rangle$ to a ground state $|\mathrm{g}\rangle$ of a quantum two-level system. The process is effected by the emission of a field quantum between the single-quantum state $|\{\mathbf{k}, k_z, \eta\}\rangle$ of frequency $\omega(k, k_z)$ and polarisation η and the vacuum state, represented by $|\{0\}\rangle$.

The steps leading to the evaluation of the de-excitation rate are straightforward, albeit a little involved mathematically. We illustrate the procedure by considering the details for the case of a dipole moment vector oriented parallel to the z-axis. We then generalise the results to obtain a closed form applicable for an arbitrary dipole orientation. Finally, we proceed to display the spatial distributions of the de-excitation rate for different dipole orientations.

3.1. Dipole oriented along the z-axis

Suppose that the dipole moment vector is oriented parallel to the z-axis, i.e. perpendicular to the x–y plane. In this case, only the transverse electric (TE) modes contribute to the emission process. Making use of Eq. (7), with Eq. (5), we have from Eq. (9)

$$\Gamma_z(x_0, y_0, 0) = \frac{2\mu^2 \bar{c}^2}{\pi^2 \varepsilon_0} \int \mathrm{d}^2 \mathbf{k} \int_{-\infty}^{\infty} \mathrm{d}k_z \frac{k^2}{\omega} \sin^2(k_x x_0) \sin^2(k_y y_0) \delta(\omega - \omega_0), \tag{10}$$

where the subscript z in Γ_z signifies the dipole orientation is the z-direction. The steps leading to the evaluation of the integrals are outlined in Appendix A. The result is

$$\Gamma_z(x_0, y_0) = \Gamma_{\text{bulk}}[1 - \mathscr{G}_z(2\mathbf{x}_0) - \mathscr{G}_z(2\mathbf{y}_0) + \mathscr{G}_z(2\mathbf{x}_0 + 2\mathbf{y}_0)], \tag{11}$$

where $\mathbf{x}_0 = \hat{\mathbf{x}}x_0$ (and similarly for $\mathbf{y}_0$) and Γ_{bulk} is given by

$$\Gamma_{\text{bulk}} = \frac{\mu^2 \omega_0^3}{3\pi\varepsilon_0 \hbar c^3} \mathscr{R}, \tag{12}$$

where $\mathscr{R}$ is a multiplicative factor accounting for the local field corrections [11–14] and, for a generic vector $\mathbf{v}$, the function $\mathscr{G}(\mathbf{v})$ is defined as

$$\mathscr{G}_z(\mathbf{v}) = \frac{\sin(K_0 v)}{K_0 v} + \left(\frac{\cos(K_0 v)}{K_0^2 v^2} - \frac{\sin(K_0 v)}{K_0^3 v^3}\right), \tag{13}$$

where $\mathbf{v}$ takes the values $2\mathbf{x}_0$, $2\mathbf{y}_0$ and $2(\mathbf{x}_0 + \mathbf{y}_0)$.

3.2. Dipole oriented in an arbitrary direction

The evaluation of the emission rate in the case of a dipole oriented at an arbitrary direction $\hat{\boldsymbol{\mu}}$ follows an analogous procedure to that outlined above for the case of a dipole along the z-axis. Appendix A proceeds to determine the expressions appropriate for a general dipole orientation. The final result for an arbitrary dipole orientation $\hat{\boldsymbol{\mu}}$ is

$$\Gamma_{\hat{\boldsymbol{\mu}}}(x_0, y_0) = \Gamma_{\text{bulk}}\left\{1 - \mathscr{G}_{\hat{\boldsymbol{\mu}}}(2\mathbf{x}_0) - \mathscr{G}_{\hat{\boldsymbol{\mu}}}(2\mathbf{y}_0) + \mathscr{G}_{\hat{\boldsymbol{\mu}}}(2\mathbf{x}_0 + 2\mathbf{y}_0)\right\}, \tag{14}$$

where

$$\mathscr{G}_{\hat{\boldsymbol{\mu}}}(\mathbf{v}) = [1 - \hat{\boldsymbol{\mu}} \cdot \hat{\mathbf{v}}]\frac{\sin(K_0 v)}{K_0 v} + [1 - 3\hat{\boldsymbol{\mu}} \cdot \hat{\mathbf{v}}]\left\{\frac{\cos(K_0 v)}{K_0^2 v^2} - \frac{\sin(K_0 v)}{K_0^3 v^3}\right\}. \tag{15}$$

It is easy to check that the general results displayed above reduce to those for the special case of a dipole along the z-axis, Eqs. (11) and (13).

4. Rate distributions

Having derived the general result in Eqs. (14) and (15), we are now in a position to explore the characteristics of the de-excitation rate to uncover the spatial distribution and orientational dependence of the interference effects, especially any superradiance and subradiance features that the physical environment might exhibit.

Fig. 2 displays the spatial distribution of the emission rate when the dipole moment vector of the emitter is oriented along the z-axis: $\boldsymbol{\mu} = (0, 0, \mu)$. Fig. 2(a) is a surface plot presenting the variation of $\Gamma/\Gamma_{\text{bulk}}$ at points (x_0, y_0) in the vicinity of the intersection line at $(0, 0)$. There are peaks, where the rate is maximum, and troughs where it is minimum, with the maximum localised at sub-wavelength distance from the intersection line. Fig. 2(b) is a contour plot in which it is clear that the region nearest to the intersection line is sub-radiant. In fact it can be shown that for small distances from the intersection line, satisfying $K_0 x_0 \ll 1$ and $K_0 y_0 \ll 1$, we have

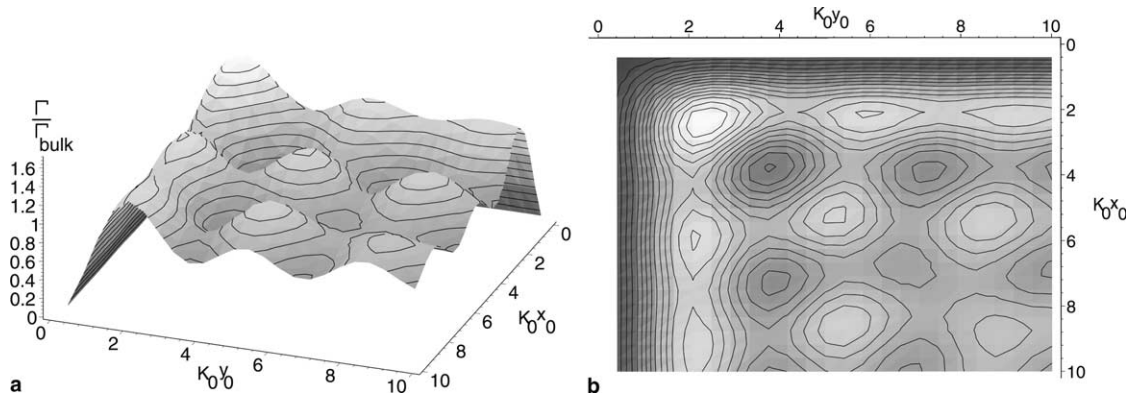$$\frac{\Gamma_z}{\Gamma_{\text{bulk}}} \approx \frac{1}{10} K_0^4 x_0^2 y_0^2. \tag{16}$$

Fig. 2. The spatial distribution of the relative emission rate $\Gamma/\Gamma_{\text{bulk}}$ when the emitter dipole moment vector is parallel to the intersection line, $\boldsymbol{\mu} = (0, 0, \mu)$. The distances x_0 and y_0 are in units of $K_0^{-1} \equiv \lambda_0/2\pi$ where λ_0 is the transition wavelength. (a) is a surface plot of the relative emission rate for points in the vicinity of the intersection line. (b) is a contour plot showing variations in the same region as in (a).

We also note from Fig. 1 that when such emitters are positioned on the symmetry line $x_0 = y_0$, they experience the highest maxima and the lowest minima of the emission rate.

Fig. 3 is also concerned with the situation discussed in Fig. 2, but here the dipole moment vector is oriented parallel to one of the conductor surfaces and perpendicular to the other. In Fig. 3(a), one sees that the region nearest to the surface to which the dipole moment vector is parallel is a region of high suppression of spontaneous emission (sub-radiance), while the corresponding region nearest to the other conductor exhibits superradiance. In fact, if the transition dipole is oriented along the xy-plane ($\hat{\mu}_z = 0$), one has

$$\Gamma_{x,y}/\Gamma_{\text{bulk}} = \frac{2K_0^2}{5} \left\{ x_0^2 \left(4 - 4|\hat{\mu}_x^2| \right) + y_0^2 \left(4 - 4|\hat{\mu}_y^2| \right) - 2x_0 y_0 \left(\hat{\mu}_x \hat{\mu}_y^* + \hat{\mu}_y \hat{\mu}_x^* \right) \right\}. \tag{17}$$

From this, we deduce that if the transition dipole is oriented along the y-axis ($\hat{\mu}_x = 0$ and $\hat{\mu}_y = 1$), one has in the small distance limit described above
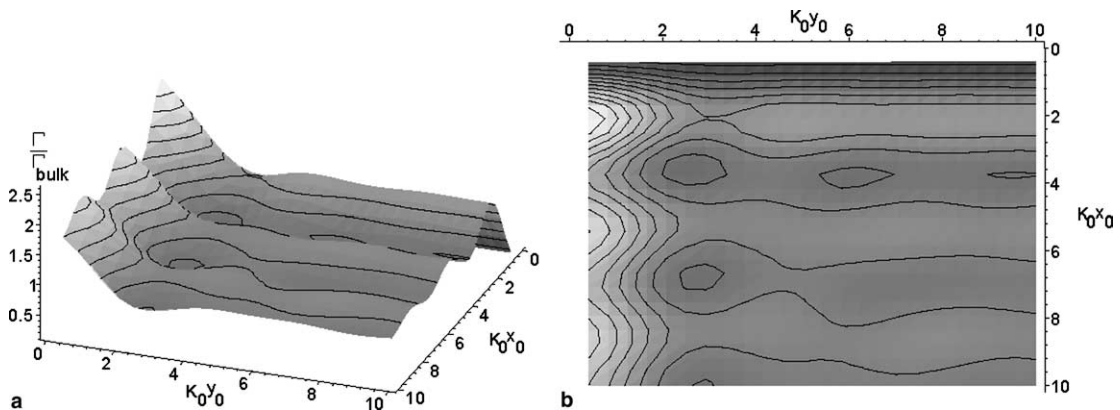

Fig. 3. As in Fig. 2(a) and (b), but here the dipole moment vector is oriented parallel to one of the conductor planes and perpendicular to the other.

$$\Gamma_{x,y}/\Gamma_{\text{bulk}} \approx \frac{8K_0^2 y_0^2}{5}. \tag{18}$$

These observations are made clearer in view of the contour plot in Fig. 3(b).

In conclusion, we have systematised the theory describing quantum interference effects predicted to be exhibited by a radiating dipolar system situated near the intersection line arising from joining the planar surfaces of two perfect conductors at a right angle. There are distinct regions where the emitter could be positioned, displaying suppression and enhancement of the emission process, depending on the dipole orientation. The above predictions should be experimentally verifiable for transitions in the optical region of the spectrum.

The results (and, in particular, those displayed in Fig. 2) indicate that the de-excitation rate goes to zero as the dipole approaches the surface. This is because our model does not accommodate non-radiative losses due to the finite conductivity of the mirrors. If the losses were included, there would be a rapid de-excitation in the vicinity of the surface due to a non-radiative (resistive) coupling to it, i.e., due to the losses at the mirrors. However, consideration of this issue goes beyond the scope of this communication and so it will not be discussed here any further.

We suggest that the physical situation we have presented here could be exploited as a basis for the design of a scalable architecture for quantum information processing. Suitable emitters, such as atoms, molecules, or quantum dots, could be positioned at well defined distances in the vicinity of the intersection line and that the orientation of their transition dipole moment vectors can be controlled, for example, optically. Our results suggest that at certain positions where the emitter can be localised, its emission could be switched on and off, simply by a change of the dipole orientation. For two identical emitters near the intersection line, the expected two-body entanglement should be modified significantly by the quantum interference when the emitters are situated near the intersection line. The two-body entanglement need not be for emitters on the same x–y plane, but the emitters could be on different planes near the intersection line and their dipole moment vectors could be oriented in arbitrary directions. Work on this relatively more complicated situation is now in progress.

Acknowledgements

Appendix A

In this Appendix, we systematise the mathematics needed to evaluate the de-excitation rates. We begin by the special case in which the dipole is oriented in the z-direction, as given in Eq. (10). For a general point $(x, y, 0)$ this can now be written as follows:

$$\Gamma_z(x, y, 0) = \frac{\mu^2 \bar{c}^2}{2\pi^2 \hbar \varepsilon_0} \int d^3 \mathbf{K} \frac{k^2}{\omega} \sin^2(k_x x) \sin^2(k_y y) \delta(\omega - \omega_0), \tag{19}$$

where we have introduced the three-dimensional wavevector $\mathbf{K} = (\mathbf{k}, k_z)$. The integration over $\mathbf{K}$ spans the intervals $-\infty < k_z < \infty$ and $0 < k_x, k_y < \infty$. Since the integrand is an even function, we may extend the k_x, k_y integrations to be $-\infty < k_x, k_y < \infty$ and use spherical polar coordinates in $\mathbf{K}$ space to write $d^3 \mathbf{K} = K^2 dK d\Omega$, where Ω is an element of the solid angle. We then have

$$\Gamma_z(x,y,0) = \frac{\mu^2}{2\hbar\pi^2\varepsilon_0} \int_0^\infty K^3 \, \mathrm{d}K \int \mathrm{d}\Omega (1-\hat{k}_z^2)\sin^2(k_x x)\sin^2(k_y y)\delta(K-K_0), \tag{20}$$

where $\hat{k}_z = k_z/K$ and we have used $\omega = \bar{c}K$. We may then carry out the K-integration to obtain

$$\Gamma(x,y,0) = \frac{\mu^2 K^3}{3\varepsilon_0\hbar\pi} \mathscr{I}(x,y)|_{K=K_0=\omega_0/\bar{c}}, \tag{21}$$

where

$$\mathscr{I}(x,y) = \frac{3}{2\pi} \int \mathrm{d}\Omega (1-\hat{k}_z^2)\sin^2(k_x x)\sin^2(k_y y). \tag{22}$$

The next step is to evaluate the integral $\mathscr{I}$. First it is easy to show that we have

$$\sin^2(k_x x)\sin^2(k_y y) = \frac{1}{4}\left\{ 1 - \cos(2k_x x) - \cos(2k_y y) + \frac{1}{2}\cos(2k_x x + 2k_y y) + \frac{1}{2}\cos(2k_x x - 2k_y y) \right\}. \tag{23}$$

In the final term, one can make the replacement $k_y \to -k_y$. This does not change the result because the corresponding integrand term is symmetric and the integration is over all angles. Thus, we can write

$$\sin^2(k_x x)\sin^2(k_y y) \to \frac{1}{4}\left\{ 1 - \cos(2k_x x) - \cos(2k_y y) + \cos(2k_x x + 2k_y y) \right\}. \tag{24}$$

The $\mathscr{I}_z$ integral can now be cast in the form

$$\mathscr{I}_z(x,y) = \frac{3}{8\pi} \int \mathrm{d}\Omega (1-\hat{k}_z^2)[1 - \cos(2\mathbf{K}\cdot\mathbf{x}) - \cos(2\mathbf{K}\cdot\mathbf{y}) + \cos(2\mathbf{K}\cdot(\mathbf{x}+\mathbf{y}))]. \tag{25}$$

Now introducing the generic integral

$$\mathscr{G}_z(\mathbf{v}) = \frac{3}{8\pi} \int \mathrm{d}\Omega (1-\hat{k}_z^2)\cos(\mathbf{K}\cdot\mathbf{v}), \tag{26}$$

we can then write

$$\mathscr{I}_z(x,y) = \mathscr{G}_z(\mathbf{0}) - \mathscr{G}_z(2\mathbf{x}) - \mathscr{G}_z(2\mathbf{y}) + \mathscr{G}_z(2\mathbf{x}+2\mathbf{y}). \tag{27}$$

That the first term in Eq. (25) is in fact unity can be seen immediately. We have

$$\mathscr{G}_z(\mathbf{0}) = \frac{3}{8\pi} \int \mathrm{d}\Omega (1-\hat{k}_z^2) = \frac{3}{8\pi}\frac{2}{3} \int \mathrm{d}\Omega = 1. \tag{28}$$

Consider now the general case involving a dipole oriented in an arbitrary direction. Instead of Eq. (27) we have

$$\mathscr{I}_{\hat{\boldsymbol{\mu}}}(x,y) = \sum_{i,j} \hat{\mu}_i \mathscr{G}_{ij}(\mathbf{v})\hat{\mu}_j, \tag{29}$$

where $\hat{\mu}_i$ is the ith Cartesian vector component of the unit vector along the dipole moment vector $\boldsymbol{\mu}$, while the tensor $\mathscr{G}_{ij}$ is the generalisation of the integral related to Eq. (26)

$$\mathscr{G}_{ij}(\mathbf{v}) = \frac{3}{8\pi} \int \mathrm{d}\Omega [\delta_{ij} - \hat{K}_i\hat{K}_j]\cos(\mathbf{K}\cdot\mathbf{v}). \tag{30}$$

The integration can be carried out to yield

$$\mathscr{G}_{ij}(\mathbf{v}) = \alpha_{ij}\frac{\sin(K_0 v)}{K_0 v} + \beta_{ij}\left\{ \frac{\cos(K_0 v)}{K_0^2 v^2} - \frac{\sin(K_0 v)}{K_0^3 v^3} \right\}, \tag{31}$$

where

$$\alpha_{ij}(\mathbf{v}) = \delta_{ij} - \hat{v}_i\hat{v}_j; \quad \beta_{ij}(\mathbf{v}) = \delta_{ij} - 3\hat{v}_i\hat{v}_j. \tag{32}$$

On substituting for $\mathscr{G}_{ij}$ in Eq. (29), we have

$$\Gamma_{\hat{\boldsymbol{\mu}}}(x,y) = \Gamma_{\text{bulk}}\big\{1 - \mathscr{G}_{\hat{\boldsymbol{\mu}}}(2\mathbf{x}) - \mathscr{G}_{\hat{\boldsymbol{\mu}}}(2\mathbf{y}) + \mathscr{G}_{\hat{\boldsymbol{\mu}}}(2\mathbf{x} + 2\mathbf{y})\big\}, \tag{33}$$

where

$$\mathscr{G}_{\hat{\boldsymbol{\mu}}}(\mathbf{v}) = [1 - \hat{\boldsymbol{\mu}}\cdot\hat{\mathbf{v}}]\frac{\sin(K_0 v)}{K_0 v} + [1 - 3\hat{\boldsymbol{\mu}}\cdot\hat{\mathbf{v}}]\left\{\frac{\cos(K_0 v)}{K_0^2 v^2} - \frac{\sin(K_0 v)}{K_0^3 v^3}\right\}, \tag{34}$$

which is the result quoted in Eq. (15).

References

[1] E.M. Purcell, Phys. Rev. 69 (1946) 681.
[2] K.H. Drexhage, J. Lumin. 1–2 (1970) 693;
E. Wolf (Ed.), Progress in Optics XII, North Holland, Amsterdam, 1974, 165p.
[3] J. Michaelis, C. Hettich, J. Mlynek, V. Sandoghdar, Nature 405 (2000) 325.
[4] D. Bouwmeester, A. Ekert, A. Zelinger (Eds.), The Physics of Quantum Information, Springer, Berlin, 2000.
[5] A. Beveratos, R. Brouri, T. Cacoin, J.-P. Poizat, P. Grangier, Phys. Rev. A64 (2001) 061802(R).
[6] A. Beveratos, R. Brouri, T.J.-P. Poizat, P. Grangier, Opt. Lett. 25 (2000) 1294.
[7] D. Jaksch, J.I. Cirac, P. Zoller, S.R. Rolston, R. Cote, M.D. Lukin, Phys. Rev. Lett. 85 (2000) 2208.
[8] T. Calarco, A. Datta, P. Fedichev, E. Pazy, P. Zoller, Phys. Rev. A68 (2003) 012310.
[9] U. Dorner, P. Fedichev, D. Jaksch, M. Lewinstein, P. Zoller, Phys. Rev. Lett. 91 (2003) 073601.
[10] M. Al-Amri, M. Babiker, Phys. Rev. A67 (2003) 043820;
M. Al-Amri, M. Babiker, Phys. Rev. A69 (2004) 065801.
[11] R.J. Galuber, M. Lewenstein, Phys. Rev. A43 (1991) 467.
[12] S.M. Barnett, in: S. Raynaud, E. Giacobino, Zinn-Justin (Eds.), 'Quantum Fluctuations', Les Houches Lectures, Session 62, North-Holland, Amsterdam, 1997.
[13] P. de Vries, A. Lagendijk, Phys. Rev. Lett. 81 (1998) 1381.
[14] G. Juzeliunas, D.L. Andrews, Adv. Chem. Phys. 112 (2000) 357.